Journal of Solid State Chemistry 184 (2011) 3324–3328

Contents lists available at SciVerse ScienceDirect

Journal of Solid State Chemistry

journal homepage: www.elsevier.com/locate/jssc

Excellent red phosphors of double perovskite Ca_2LaMO_6:Eu (M=Sb, Nb, Ta) with distorted coordination environment

Xin Yin [a], Yaoming Wang [a], Fuqiang Huang [a,b,*], Yujuan Xia [1,a], Dongyun Wan [a], Jiyong Yao [c,**]

[a] State Key Laboratory of High Performance Ceramics and Superfine Microstructures and CAS Key Laboratory of Materials for Energy Conversion, Shanghai Institute of Ceramics, Chinese Academy of Sciences, Shanghai 200050, PR China
[b] College of Chemistry and Molecular Engineering, Peking University, Beijing 100871, PR China
[c] Key Laboratory of Functional Crystals and Laser Technology, Technical Institute of Physics and Chemistry, Chinese Academy of Sciences, Beijing 100190, PR China

ARTICLE INFO

Article history:
Received 28 July 2011
Received in revised form
9 October 2011
Accepted 17 October 2011
Available online 25 October 2011

Keywords:
Double perovskite structure
Red luminescence
Quantum efficiency

ABSTRACT

Double perovskite Ca_2LaSbO_6, successfully synthesized by solid state reaction method, was identified by Rietveld refinements to crystallize in the monoclinic space group $P2_1/n$, which is isostructural to Ca_2LaMO_6 (M=Nb, Ta). Excellent red luminescence of Eu-doped Ca_2LaMO_6 (M=Sb, Nb, Ta) can be obtained and no luminescence quenching effect was observed when Eu-doping level reached 40%. For $Ca_2La_{0.6}NbO_6$:$0.4Eu^{3+}$, quantum efficiencies of 20.9% and 27.7% were reached to show high light conversion and bright red emission excited at 465 nm (blue light) and 534 nm (green light), respectively, comparable to the commercial phosphors. Through systemic investigation for the series of double perovskite compounds, the excellent red emission in Ca_2LaMO_6 is attributed to highly distorted polyhedra of EuO_8 (low tolerance factor of the pervoskite), and large bond distances of La–O (low crystal field effect of the activator).

1. Introduction

The development of efficient white light emitting diodes (WLEDs) based on III–V wide bandgap semiconductors has led to the considerable progress in the field of solid state lighting with high efficiency, good reliability and long lifetime. As an indispensable component, phosphors play a key role in WLEDs. The commonly used combination of blue chips with yellow phosphors ($Y_3Al_5O_{12}$:Ce^{3+}) suffers from undesirably low color rendering index and high color temperature which red phosphors are demanded to adjust [1]. The commercial red phosphors of sulfides are unstable and oxynitrides and nitrides need rigorous synthesis conditions. For example, Y_2O_2S:Eu usually undergoes degradation under high current densities in the application of field emission display technology [2]. For $Sr_2Si_5N_8$:Eu, the synthesis processes are usually under higher temperature (>1600 °C) and need the N_2 gas atmosphere to prevent oxidization [3]. Therefore, the oxide-based red phosphors are desirable [4–7].

Luminescent properties of phosphor materials are tightly correlated to the motions of energy carriers (electron, photon, and phonon), and the energy transfer is the central issue [8]. Due to relatively easy energy transfer when B site is occupied by the transition metal, most of perovskites ABO_3 are not good phosphors, although they are very stable, such as $CaZrO_3$:Eu^{3+} [9]. The ordered double perovskites A_2LnMO_6 (A=alkaline earth metal; Ln=rare earth element; M=transition metal, d-block metal), which can be structurally modulated with an abundant of elements, concentrate lots of interests [10–13] and may be suitable candidate phosphors. The alternative arrangement of octahedron LnO_6 (AO_6) and MO_6 in A_2LnMO_6 can reduce the symmetry of A sites and contribute a variety of environments for dopants.

With these considerations, we have synthesized a series of double-perovskite compounds A_2LnMO_6 (A=Ca, Sr, Ba; Ln=La, Gd, Y; M=Sb, Nb, Ta) by conventional solid state reaction method. By doping Eu^{3+} ions, the intense red emission was successfully excited by blue light (465 nm) to match blue InGaN chips, and high quantum efficiency is achieved with an optimal doping content up to 40%.

2. Experiments

2.1. Sample preparation

Polycrystalline powder samples A_2LnMO_6:Eu (A=Ca, Sr, Ba; Ln=La, Gd, Y; M=Sb, Nb, Ta), as well as $SrZrO_3$:$Eu^{3+}Li^{+}$,

* Corresponding author at: State Key Laboratory of High Performance Ceramics and Superfine Microstructures and CAS Key Laboratory of Materials for Energy Conversion, Shanghai Institute of Ceramics, Chinese Academy of Sciences, Shanghai 200050, PR China. Fax: +86 21 5241 6360.
** Corresponding author. Fax: +86 10 6255 4670.
E-mail addresses: huangfq@mail.sic.ac.cn (F. Huang), jyao@mail.ipc.ac.cn (J. Yao).
[1] Present address: China National Institute of Standardization, Zhichun Road, Haidian District, Beijing, PR China. Fax: 010 58811714.

0022-4596/$ - see front matter © 2011 Elsevier Inc. All rights reserved.
doi:10.1016/j.jssc.2011.10.032

$LaAlO_3:Eu^{3+}$ and $Sr_2Ca(Mo_{0.1}W_{0.9})O_6:Eu^{3+}Li^+$ for comparison, were obtained by conventional solid state reaction starting from $CaCO_3$, $SrCO_3$, $BaCO_3$, La_2O_3, Gd_2O_3, Y_2O_3, Sb_2O_3, Nb_2O_5, Ta_2O_5, ZrO_2, Al_2O_3, MoO_3, WO_3, and Eu_2O_3. All the reagents were purchased from Sinopharm Chemical Reagent Co. Ltd. with the purity of 99.99% and used as-received. In a typical procedure, stoichiometric amounts of all the reagents were ground and mixed thoroughly in an agate mortar. Then the mixture was transferred into the crucible and precalcined at 1000 °C in the electric stove. For A_2LnSbO_6, the mixture is precalcined at 625 °C to ensure the full oxidization of Sb^{3+} to Sb^{5+} and then at 1000 °C. Subsequently, the mixture was reground and calcined at 1400 °C for 24 h for the complete reaction.

2.2. Characterization

Powder X-ray diffraction patterns were collected at room temperature on a Bruker D8 Focus diffractometer using Cu $K\alpha$ radiation with the scanning speed of 12°/min in the range of 5–85°. The XRD data for the Rietveld refinement was recorded with the scanning speed of 0.1°/min and the range of 10–85° on the same diffractometer. Rietveld refinements were performed with EXPGUI and GSAS program packages [14,15]. The refined parameters include the scale factor, the terms for background function, unit cell parameters, zero point error, profile coefficients, atomic positions, isotropic displacement parameters, and the phase fraction. The excitation and emission spectra of the samples were recorded on a Horiba Jobin Yvon Fluoromax-4 Spectrofluorometer. The measurement was performed at room temperature using the excitation wavelength of 465 nm and the emission wavelength of 615 nm. Quantum efficiencies were obtained from this setup with the integrating sphere and the spreadsheet of ISO PLQY Calculator.

3. Results and discussion

3.1. Crystal structure

The crystal structure of Ca_2LaSbO_6 was determined by the powder X-ray diffraction. The refined results for Ca_2LaSbO_6 are shown in Table S1 of Supplementary Materials in detail, which agree well with Faik's refined results. Ca_2LaSbO_6 crystallizes in the space group $P2_1/n$ with cell constants of $a=5.6852(1)$ Å, $b=5.8781(1)$ Å, $c=8.1723(1)$ Å, and $\beta=89.99(4)°$. As shown in Fig. 1b, the crystal structure contains six unique crystal sites (Ca1, Ca2, Sb, O1, O2, O3), where the Ca1 site is occupied by the disordered 50% Ca and 50% La. Ca_2LaSbO_6 can be denoted as $(Ca_{1/2}La_{1/2})_2CaSbO_6$ to follow the typical double perovskite A_2B1B2O_6 ($A=Ca_{1/2}La_{1/2}$, $B1=$Ca, $B2=$Sb). The large differences of ionic radii and oxidation state between Ca^{2+} (1.00 Å) and Sb^{5+} (0.60 Å) result in the ordering of $B1$ (Ca) and $B2$ (Sb). Both of the cations are arranged alternately and have a rock salt sublattice. The selected bond distances of Ca_2LaSbO_6 are listed in Table S2. The Sb atom is in the center of the octahedral SbO_6 (Sb–O: 2.00(8)–2.07(8) Å). The Ca2 atom is octahedrally coordinated to six O atoms, and the Ca2–O bond distances range from 2.222(9) to 2.288(9) Å, as shown in Fig. 1d. The Ca1 (La) atom is located in a highly distorted polyhedron surrounded by eight O atoms (Fig. 1c), which is evident by much larger deviation of Ca1(La)–O bond distances (2.38(1)–2.97(1) Å) than that of Ca2–O in the $Ca2O_6$ octahedron. It is also reasonable for the larger La^{3+} (1.16 Å) to occupy an eight-coordination cavity. Both $Ca2O_6$ and SbO_6 have an inversion center, but $Ca1O_8$ does not. In $Ca_2La_{1-x}SbO_6:xEu^{3+}$, the doping Eu^{3+} atoms mainly occupy at the eight-coordinated Ca1 site, and very small amount of Eu^{3+} may go to the six-coordinated Ca2 site due to the ionic radius of Eu^{3+} (0.95 Å) close to Ca^{2+} (1.00 Å).

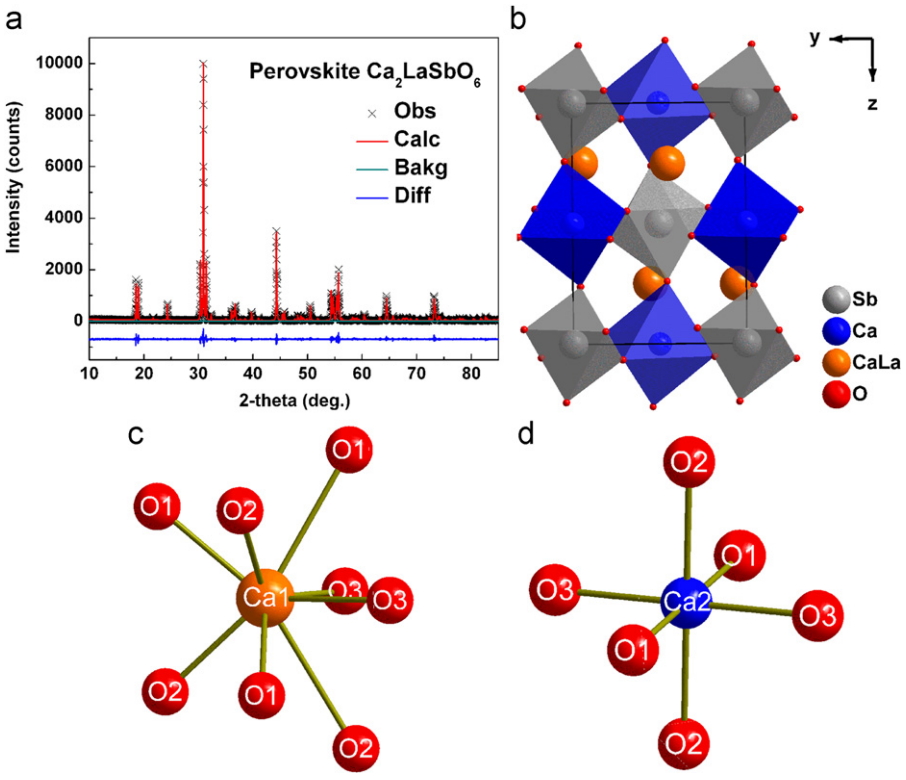

Fig. 1. (a) Rietveld refinement results of double perovskite Ca_2LaSbO_6. (b) Crystal structure of Ca_2LaSbO_6 viewed along [1 0 0]. (c) Highly distorted polyhedron $Ca1O_8$ (Ca1: 50% Ca+50% La) and (d) octahedron $Ca2O_6$.

The structure of Sr_2LaSbO_6 (A_2B1B2O_6: A=Sr, $B1$=La, $B2$=Sb) is different from that of Ca_2LaSbO_6, which can be derived from the crystal structure of Ca_2LaSbO_6. The Sr atom prefers to occupy the Ca1 site of Ca_2LaSbO_6 to form a highly distorted polyhedron SrO_8, and the La atom is at the Ca2 site to form LaO_6 instead of LaO_8. It is easy to understand the structure difference between Ca_2LaSbO_6 and Sr_2LaSbO_6 from the different ionic radii of Ca^{2+} (1.12 Å), Sr^{2+} (1.26 Å), and La^{3+} (1.16 Å). Larger cations enter into larger coordination environments. The La atoms in Ca_2LaSbO_6 are mainly at the larger Ca1 site instead of the Ca2 site, and the La atoms in Sr_2LaSbO_6 have to occupy at the octahedral site. Sr_2GdSbO_6 and Ba_2LaSbO_6 (space group: $P2_1/n$) is isostructural to Sr_2LaSbO_6. But Sr_2YSbO_6 and Ba_2LnSbO_6 (Ln=Gd, Y) crystallize in the cubic system with the space group of Fm-3m, and the basic crystal structure and the coordination environments of La and Sb are similar to Sr_2LaSbO_6. In A_2LnSbO_6:Eu^{3+} (A=Sr, Ba), the doping Eu^{3+} atoms prefer to occupy at the six-coordinated Ln site.

The XRD patterns of $Ca_2La_{1-x}SbO_6$:xEu^{3+} (x=0, 0.12, 0.35, 0.75, 1) are shown in Fig. 2a. The samples possess the same monoclinic double perovskite structure as Ca_2LaSbO_6, and no impurity peaks were observed. The peak gradually moves slightly towards the higher diffraction angle with increasing x (e.g. the enlarged XRD patterns ranging from 43.5° to 46.5° are shown in the right part of Fig. 2a), which is consistent with the solubility of the smaller Eu^{3+} ions in the host lattice.

3.2. Luminescence properties

The room temperature excitation spectra of $Ca_2La_{1-x}SbO_6$:xEu^{3+} (x=0–1) monitored at 615 nm were performed, as shown in Fig. 2b (e.g. x=0.40). The broad band around 300 nm is attributed to the overall combination of charge transfer transition in metal−oxygen polyhedron of the compound [7]. Several sharp peaks at visible range such as 395 nm, 465 nm, and 534 nm are from Eu^{3+} ions characteristic inner-4f transitions, $^7F_0 \rightarrow {}^5L_6$, $^7F_0 \rightarrow {}^5D_2$, $^7F_0 \rightarrow {}^5D_1$, respectively. It indicates that the Eu-doped samples can be excited by violet light, blue light, and green light. Excited at 465 nm, intense red emission was obtained from the transitions $^5D_0$ to ^7F_J (J=0–2) (Fig. 2c). Being different from many reported luminescence materials excited by ultraviolet or near-ultraviolet light [16–18], the double-perovskite phosphor can be excited by blue light, matching well with the emission wavelength of the blue chips (e.g. InGaN) utilized currently in LED devices.

The inset of Fig. 2c displays the relationship between red emission intensity at 615 nm and Eu^{3+} ions concentration. The emission intensity increases with increasing the Eu^{3+} doping content and declines at $x > 0.4$. The upslope at $0 < x \leq 0.4$ is due to the increase in the optical active centers (Eu^{3+}). Compared with the other Eu-doped phosphors [3–5,19], the optimal doping content up to x=0.4 in Ca_2LaSbO_6 is unique, indicating a weak non-radiative energy transfer between Eu^{3+} pairs. The critical Eu^{3+}…Eu^{3+} distance (R) can be calculated from $R=2(3V/(4\pi x_c N))^{1/3}$ [20], where x_c is the optimal doping content, N is the number of total Ln^{3+} sites per unit cell, and V is the volume of unit cell. Using x_c=0.4, N=2, and V=273.11 Å^3, the critical distance is determined to be ~8.67 Å. At this distance, both the exchange and multipolar interaction exist for the energy transfer. Taking the simple perovskite $SrZrO_3$:0.2Eu^{3+},0.2Li^+ for comparison (x_c=0.03, V=285.24 Å^3, N=4) [21,22], the critical distance is about 16.56 Å, much larger than in Ca_2LaSbO_6. This indicates the

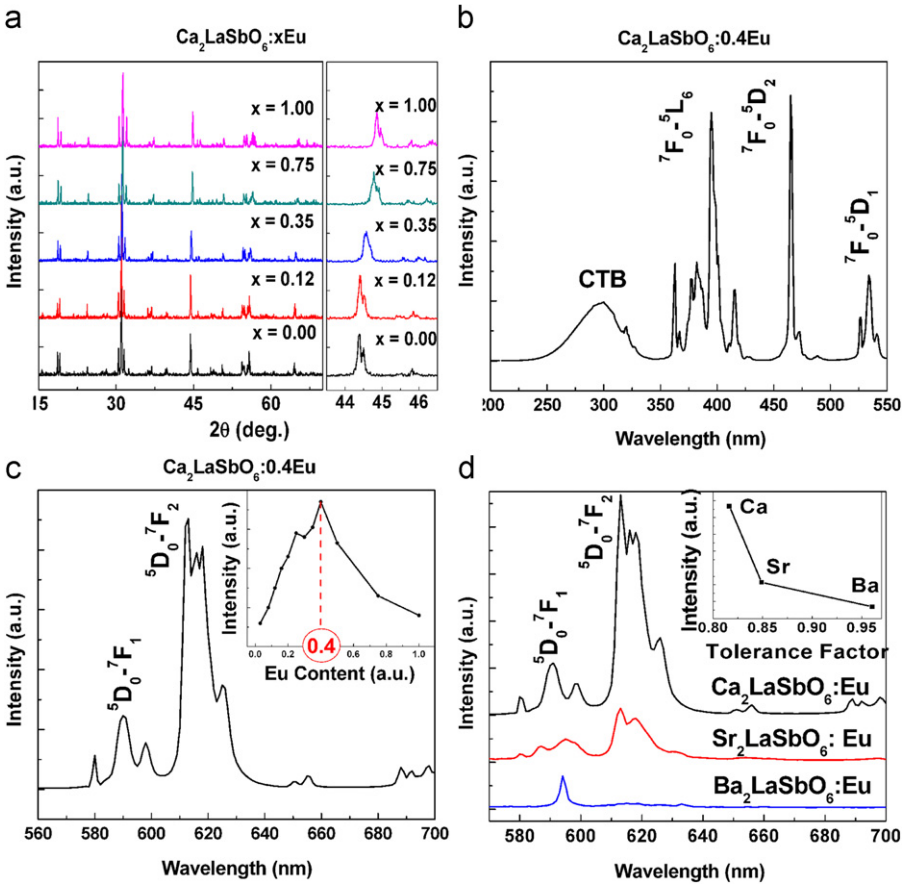

Fig. 2. (a) XRD patterns of $Ca_2La_{1-x}SbO_6$:xEu^{3+} (x=0, 0.12, 0.35, 0.75, 1) in the left side, and enlarged XRD patterns from 43.5° to 46.5° in the right side. (b) Excitation spectrum (λ_{em}=615 nm) of $Ca_2La_{0.6}SbO_6$:0.4Eu^{3+}. (c) Emission spectrum (λ_{ex}=465 nm) of $Ca_2La_{0.6}SbO_6$:0.4Eu^{3+}, and the plot of the intensity from $^5D_0 \rightarrow {}^7F_2$ versus Eu^{3+} doping content in the inset. (d) Emission spectra of $A_2La_{0.6}SbO_6$:0.4Eu^{3+} (A=Ca, Sr, Ba) excited by 465 nm, and the plot of the intensity versus tolerance factor in the inset.

energy transfer in such simple perovskites can be easily occurred even when the distance between Eu^{3+} ions pairs is much larger. Due to the strong energy transfer, the emission intensity of these simple perovskite compounds of both $Sr_{0.6}ZrO_3$:$0.2Eu^{3+}$,$0.2Li^+$ and $LaAlO_3$:$0.2Eu^{3+}$ [23] is much lower, as shown in Figure S1 of Supplementary Materials. The higher doping level in the double perovskite may be due to the specially distorted environment formed by the orderly alternative arrangement of octahedron $Ca2O_6$ and SbO_6.

The emission spectra of $A_2La_{0.6}SbO_6$:$0.4Eu^{3+}$ (A=Ca, Sr, Ba) are displayed in Fig. 2d. For the activator of Eu^{3+}, the magnetic dipole transition $^5D_0 \rightarrow {}^7F_1$ occurs near 594 nm, and the electric dipole transition $^5D_0 \rightarrow {}^7F_2$ is near 615 nm. The emission intensity is normally hypersensitive to the crystal environment of Eu^{3+} ions [24,25]. The evolution of the emission ratio $(^5D_0 \rightarrow {}^7F_2)/(^5D_0 \rightarrow {}^7F_1)$ depends on the variation of Eu^{3+} ions site symmetry. When the emission ratio is more than 2:1 the emission transition is mainly $^5D_0 \rightarrow {}^7F_2$ (615 nm) from the Eu^{3+} sites without inversion symmetry, otherwise, when the ratio is less than 2:1 the transition is mainly from $^5D_0 \rightarrow {}^7F_1$ (594 nm) with inversion symmetry [6,26]. The ratios in $A_2La_{0.6}SbO_6$:$0.4Eu^{3+}$ (A=Ca, Sr, Ba) are 2.2:1, 1.4:1, and 0.18:1, respectively, consistent with the doped Eu^{3+} located at eight-coordinated sites (EuO_8) in $Ca_2La_{0.6}Eu_{0.4}SbO_6$ and at the six-coordinated sites (EuO_6) in $A_2La_{0.6}SbO_6$:$0.4Eu^{3+}$ (A=Sr, Ba). The doped Eu^{3+} ions at highly distorted eight-coordinated sites can rapidly promote the probability of the electric dipole transition to emit intensely red light.

In order to explore the correlation between red emission intensity and crystal structure, the tolerance factors of the double perovskites were calculated, as listed in Table S3. Tolerance factor of A_2LnMO_6, $t=(r_A+r_O)/\sqrt{2}(r_{(Ln,M)}+r_O)$, is employed to represent the structure distortion degree of the perovskite structure [27]. The inverse relation between the brightest red emission intensity and tolerance factor for A_2LaSbO_6:xEu^{3+} (A=Ca, Sr, Ba) is shown in the inset of Fig. 2d. The emission intensity increases as the tolerance factor decreases, and the brightest Ca_2LaSbO_6 has the lowest value (0.8165) among the three Sb samples. The lower tolerance factor reflects the larger distortion of the crystal structure, which corresponds to the weaker energy transfer in the framework of B-site and oxygen atoms.

The other similar double perovskites of A_2LnMO_6:$0.4Eu^{3+}$ (A=Ca, Sr, Ba; Ln=La, Gd, Y; M=Sb, Nb, Ta) were also investigated in details, shown in Fig. 3a. Their luminescent properties are similar to A_2LaSbO_6:xEu^{3+} (A=Ca, Sr, Ba). The ratio of emission transitions is directly related to the site symmetry of Ln^{3+}, where the luminescent activators of Eu^{3+} are mainly located. The Ln^{3+} atoms in Ca_2LnMO_6 are mainly occupied at the A sites of A_2B1B2O_6, but in Sr_2LnMO_6 and Ba_2LnMO_6 at the $B1$ sites [28–30]. Therefore, in the series of A_2LnMO_6:$0.4Eu^{3+}$ (A=Ca, Sr, Ba), the Ca-contained samples have more intense emission than the other respective Sr or Ba ones, as shown in Fig. 3a. In the series of A_2LnMO_6:$0.4Eu^{3+}$ (Ln=La, Gd, Y), the largest emission intensity trends to be ordered by La > Gd > Y, and the Nb samples have brighter red emission than the respective Ta or Sb ones. Among all of the investigated samples, Ca_2LaNbO_6:$0.4Eu^{3+}$ is the brightest phosphor.

Luminescence intensity at 615 nm versus average $Ln-O$ bond distance in $Ln-O$ polyhedra presenting the local size of the doping sites was plotted in Fig. 3b. For niobates, tantalates and antimonates, respectively, luminescence intensity increases with the bond distance. The larger bond distance corresponds to higher emission intensity. The phenomenon can be attributed to the crystal field effect. Apparently, the strong crystal field effect (short $Ln-O$ bond) could favor the energy transfer, which harms the luminescence intensity from the Eu^{3+} $4f$–$4f$ emission.

In order to accurately evaluate the luminescent properties of the double perovskite phosphors, quantum efficiencies of selected samples $Ca_2La_{0.6}NbO_6$:$0.4Eu^{3+}$ and $Ca_2La_{0.6}SbO_6$:$0.4Eu^{3+}$ were calculated according to the method described by de Mello [31] and Palsson [32]. The traditional red-emitting phosphors of $Sr_2Ca_{0.8}Mo_{0.1}W_{0.9}O_6$:$0.1Eu^{3+}$$0.1Li^+$ [16], Eu_2O_3, commercial red phosphor $Sr_2Si_5N_8$:Eu^{2+}, and commercial yellow phosphor $Y_3Al_5O_{12}$:Ce^{3+} were investigated as the reference samples by the same method to obtain quantum efficiency. As listed in Table 1, the quantum efficiencies of Ca_2LaNbO_6:$0.4Eu^{3+}$ are 17.8% (excited by 395 nm), 20.9% (466 nm), and 27.7% (534 nm). It indicates that Ca_2LaNbO_6:$0.4Eu^{3+}$ can be excited by near-UV, blue, and green lights. Especially the value at blue light region (465 nm) is 20.9%, comparable with commercial red nitride phosphor $Sr_2Si_5N_8$:Eu^{2+} (18.4%). Compared with the reference phosphors, $Ca_2La_{0.6}NbO_6$:$0.4Eu^{3+}$ and $Ca_2LaSb_{0.6}O_6$:$0.4Eu^{3+}$ have shown the superiority for high quantum efficiencies.

Table 1
Quantum efficiencies of Ca_2LaMO_6:$0.4Eu^{3+}$ (M=Sb, Nb) and the references at different excitation wavelength.

Samples	Excitation wavelength (nm)		
	395	465	534
Ca_2LaNbO_6:$0.4Eu^{3+}$	17.8%	20.9%	27.7%
Ca_2LaSbO_6:$0.4Eu^{3+}$	12.6%	16.6%	16.2%
$Sr_2Ca_{0.8}Mo_{0.1}W_{0.9}O_6$:$0.1Eu^{3+}$$0.1Li^+$	3.60%	7.60%	8.60%
Eu_2O_3	1.00%	1.40%	1.50%
$Sr_2Si_5N_8$:Eu^{2+}	–	18.4% [a]	–
$Y_3Al_5O_{12}$:Ce^{3+}	–	38.4% [b]	–

[a] Commercial red phosphor.
[b] Commercial yellow phosphor and the emission wavelength is 530 nm.

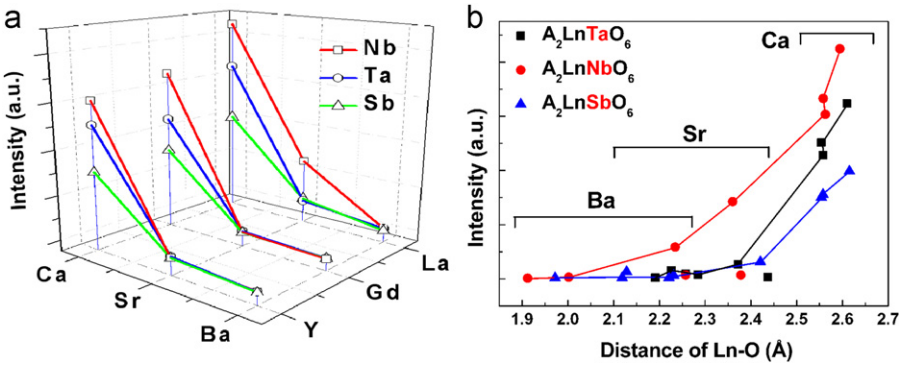

Fig. 3. (a) Relationship between highest luminescence intensity excited by 465 nm and the comprised elements of A_2LnMO_6:$0.4Eu^{3+}$ (A=Ca, Sr, Ba; Ln=La, Gd, Y; M=Sb, Nb, Ta). (b) Relationship between luminescence intensity and $Ln-O$ bond distance in $Ln-O$ polyhedra.

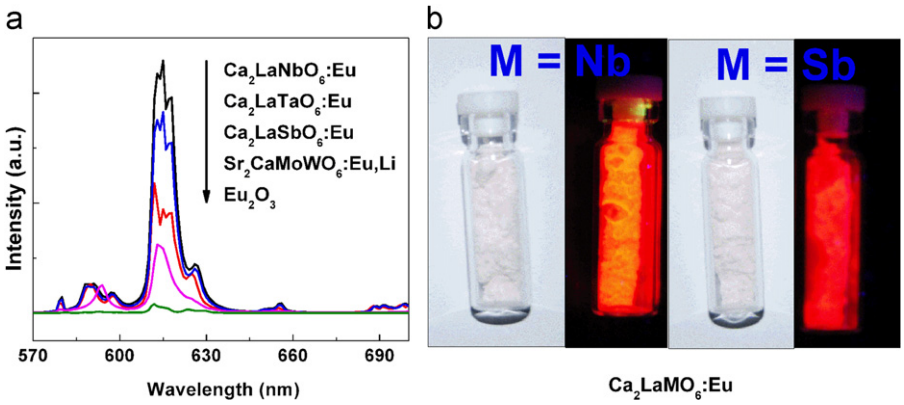

Fig. 4. (a) Luminescent spectra of $Ca_2La_{0.6}MO_6$:0.4Eu^{3+} (M =Sb, Nb, Ta), $Sr_2Ca_{0.8}Mo_{0.1}W_{0.9}O_6$:0.1$Eu^{3+}0.1Li^+$, and Eu_2O_3 excited at 465 nm. (b) Optical images of Ca_2LaMO_6:0.4Eu^{3+} (M=Nb, Sb) irradiated under a UV lamp.

The emission spectra of $Sr_2Ca_{0.8}Mo_{0.1}W_{0.9}O_6$:0.1$Eu^{3+}$,0.1$Li^+$ and Eu_2O_3 together with $Ca_2La_{0.6}MO_6$:0.4Eu^{3+} (M=Sb, Nb, Ta) are shown in Fig. 4a. The luminescence intensity of $Ca_2La_{0.6}Eu_{0.4}NbO_6$ is much higher than the others. The optical images of Ca_2LaMO_6 (M=Sb, Nb) in Fig. 4b provide direct evidence that the luminescent property of the double-perovskite compounds emit the intense orange-red light, superior to the references.

4. Conclusion

In conclusion, double perovskite Ca_2LaSbO_6 was synthesized by the solid state reaction method and refined by Rietveld method. Eu^{3+}-doped Ca_2LaMO_6 (M=Sb, Nb, Ta) phosphors possess excellent red luminescent emission, which can be excited by near-UV, blue, and green light. The intense emission transition ($^5D_0 \rightarrow {}^7F_2$) results from the highly distorted eight-coordinated sites (EuO_8) with low site symmetry presented by the tolerance factor, and the larger local size at doping site. $Ca_2La_{0.6}Eu_{0.4}NbO_6$ exhibited rather bright red emission and very high quantum efficiencies of 20.9% and 27.7% excited by blue (460 nm) and green (534 nm) light respectively, comparable to the commercial red phosphors. The new finding may make the phosphors be very promising materials for white light LED and other optical applications.

Acknowledgments

This work was financially supported by National 973/863 Program of China Grant nos. 2009CB939903 and 2011AA050505, NSF of China Grant nos. 91122034, 50821004, 21101164, 61076062, 51102263, and 61106088, and Science and Technology Commission of Shanghai Grant nos. 10520706700 and 10JC1415800.

Appendix A. Supplementary materials

Supplementary materials associated with this article can be found in the online version at doi:10.1016/j.jssc.2011.10.032.

References

[1] A.A. Setlur, W.J. Heward, Y. Gao, A.M. Srivastava, R.G. Chandran, M.V. Shankar, Chem. Mater. 18 (2006) 3314–3322.
[2] S.S. Yi, J.S. Bae, B.K. Moon, J.H. Jeong, J.C. Park, W. Kim, Appl. Phys. Lett. 81 (2002) 3344–3346.
[3] R.J. Xie, N. Hirosaki, T. Suehiro, F.F. Xu, M. Mitomo, Chem. Mater. 18 (2006) 5578–5583.
[4] Z.L. Wang, H.B. Liang, M.L. Gong, Q. Su, Electrochem. Solid State Lett. 8 (2005) H33–H35.
[5] Y.S. Hu, W.D. Zhuang, H.Q. Ye, D.H. Wang, S.S. Zhang, X.W. Huang, J. Alloys Compd. 390 (2005) 226–229.
[6] Y.C. Chang, C.H. Liang, S.A. Yan, Y.S. Chang, J. Phys. Chem. C 114 (2010) 3645–3652.
[7] I.P. Roof, M.D. Smith, S. Park, H.C. zur Loye, J. Am. Chem. Soc. 131 (2009) 4202–4203.
[8] S. Ye, F. Xiao, Y.X. Pan, Y.Y. Ma, Q.Y. Zhang, Mater. Sci. Eng. R 71 (2010) 1–34.
[9] Y. Shimizu, S. Sakagami, K. Goto, Y. Nakachi, K. Ueda, Mater. Sci. Eng. B 161 (2009) 100–103.
[10] A. Faik, E. Iturbe-Zabalo, I. Urcelay, J.M. Igartua, J. Solid State Chem. 182 (2009) 2656–2663.
[11] P.A. Tanner, Z.F. Pan, Inorg. Chem. 48 (2009) 11142–11146.
[12] K.L. Kobayashi, T. Kimura, H. Sawada, K. Terakura, Y. Tokura, Nature 395 (1998) 677–680.
[13] Y. Tomioka, T. Okuda, Y. Okimoto, R. Kumai, K.I. Kobayashi, Y. Tokura, Phys. Rev. B 61 (2000) 422–427.
[14] B.H. Toby, J. Appl. Crystallogr. 34 (2001) 210–213.
[15] A.C. Larson, R.B.V. Dreele, Los Alamos National Laboratory Report LAUR, 1994, pp. 86–748.
[16] S. Ye, C.H. Wang, Z.S. Liu, J. Lu, X.P. Jing, Appl. Phys. B–Lasers Opt. 91 (2008) 551–557.
[17] H.H. Yang, H. Cheng, Y.G. Tang, Z.G. Lu, J. Am. Ceram. Soc. 92 (2009) 931–933.
[18] T. Igarashi, M. Ihara, T. Kusunoki, K. Ohno, T. Isobe, M. Senna, Appl. Phys. Lett. 76 (2000) 1549–1551.
[19] G. Wakefield, E. Holland, P.J. Dobson, J.L. Hutchison, Adv. Mater. 13 (2001) 1557–1560.
[20] G. Blasse, Philips Res. Repts 24 (1969) 131–144.
[21] B.J. Kennedy, C.J. Howard, B.C. Chakoumakos, Phys. Rev. B 59 (1999) 4023–4027.
[22] J.L. Huang, L.Y. Zhou, Z.L. Wang, Y.W. Lan, Z.F. Tong, F.Z. Gong, J.H. Sun, L.P. Li, J. Alloys Compd. 487 (2009) L5–L7.
[23] D. Hreniak, W. Strek, P. Deren, A. Bednarkiewicz, A. Lukowiak, J. Alloys Compd. 408 (2006) 828–830.
[24] D. Vandervort, G. Blasse, Chem. Mater. 3 (1991) 1041–1045.
[25] T. Montini, A. Speghini, L. De Rogatis, B. Lorenzut, M. Bettinelli, M. Graziani, P. Fornasiero, J. Am. Chem. Soc. 131 (2009) 13155–13160.
[26] T.R. Zhang, C. Spitz, M. Antonietti, C.F.J. Faul, Chem. Eur. J 11 (2005) 1001–1009.
[27] J.B. Philipp, P. Majewski, L. Alff, A. Erb, R. Gross, T. Graf, M.S. Brandt, J. Simon, T. Walther, W. Mader, D. Topwal, D.D. Sarma, Phys. Rev. B 68 (2003) 144431.
[28] A.A. Evdokimov, A.M. Frolov, E.V. Vasilev, Inorg. Mater. 20 (1984) 1342–1344.
[29] V.K. Trunov, L.I. Konstantinova, Y.A. Velikodnyi, A.A. Evdokimov, A.M. Frolov, Russ. J. Inorg. Chem. 26 (1981) 1738–1741.
[30] V.K. Trunov, L.I. Konstantinova, A.A. Evdokimov, Russ. J. Inorg. Chem. 28 (1983) 807–809.
[31] J.C. DeMello, H.F. Wittmann, R.H. Friend, Adv. Mater. 9 (1997) 230–232.
[32] L.O. Palsson, A.P. Monkman, Adv. Mater. 14 (2002) 757–758.